Journal of Molecular Structure 1139 (2017) 31–42

Contents lists available at ScienceDirect

Journal of Molecular Structure

journal homepage: http://www.elsevier.com/locate/molstruc

Synthesis, spectroscopic, DFT and optoelectronic studies of *2-benzylidene-3-hydroxy -1-(5,6-diphenyl-1,2,4-triazine-3-yl)hydrazine* metal complexes

A. Taha [a], A.A.M. Farag [b, c, *], O.M.I. Adly [a], N. Roushdy [d], Magdy Shebl [a], H.M. Ahmed [a]

[a] *Chemistry Department, Faculty of Education, Ain Shams University, Roxy, Cairo, 11757, Egypt*
[b] *Physics Department, Faculty of Science and Arts, Aljouf University, Saudi Arabia*
[c] *Thin Film Laboratory, Physics Department, Faculty of Education, Ain Shams University, Roxy, Cairo, 11757, Egypt*
[d] *Electronic Materials Department, Advanced Technology and New Material Institute, City for Scientific Research and Technological Applications, New Borg El Arab City, 21934, Alexandria, Egypt*

ARTICLE INFO

Article history:
Received 3 January 2017
Received in revised form
20 February 2017
Accepted 6 March 2017
Available online 7 March 2017

Keywords:
Schiff base
DFT level
Photoluminescence
Optoelectronic devices

ABSTRACT

Metal complexes of Ni(II) and Cu(II) with a new Schiff base, *2-benzylidene-3-hydroxy -1-(5,6-diphenyl-1,2,4-triazine-3-yl)hydrazine* (HBDHT) have been synthesized and characterized by elemental analysis and spectroscopic methods. The results adopt octahedral and square planar structures for Ni(II) and Cu(II) complexes, respectively with the formula, $[Ni(BDHT)(NO_3)(H_2O)_2)]\cdot H_2O$ and $[Cu(BDHT)(H_2O)](NO_3)\cdot H_2O$. The emission spectra arising from S1 state is assigned to $\pi^* \rightarrow \pi$ and LUMO→HOMO transition character for investigated molecules. Structural parameters of the synthesized compounds were calculated on the basis of DFT level implemented in the *Gaussian 09* program. The size of the prepared nano particles was obtained by scanning electron microscopy (SEM) and particle size analyzer. Analysis of the absorption coefficient near the fundamental absorption edge emphasizes two indirect allowed transitions $n \rightarrow \pi^*$ and $\pi \rightarrow \pi^*$ with energy gaps of 1.1 and 2.55 eV. The forward bias current of the prepared heterojunction shows diode-like behavior with appreciable rectification characteristics. The extracted heterojunction parameters show light dependence which supporting the achievability for the optical sensor in several optoelectronic applications.

1. Introduction

The class of the 1,2,4-triazine Schiff base complexes has remained an important compounds of research due to their simple synthesis, versatility, and diverse range of applications such as biological properties [1–10], catalysts [11–13], and promising materials for optoelectronic applications [14–17] and the design of biosensors [18]. Conjugated Schiff bases have interesting optoelectronic properties and have been used in electronics such as organic and perovskite solar cells [19,20], organic field-effect transistor (OFET) [21] and electrochromic devices [22]. Their simple and clean chemistry make them a promising candidate as a low-cost alternative to currently used conjugated materials. Schiff base chemistry is also used to prepare covalent organic framework (COFs), which can be used for gas storage [23]. In continuation of our work on the synthesis of the 1,2,4 -triazine Schiff base metal complexes [24], we report the synthesis, spectral and photoluminescence properties of Cu(II) and Ni(II) complexes of the Schiff base, *2-benzylidene-3-hydroxy -1-(5,6-diphenyl-1,2,4-triazine-3-yl) hydrazine* (HBDHT) (See Fig. 1). Moreover, DFT calculations and morphological properties of prepared thin films were investigated by scanning electron microscopy (SEM). In addition, optical dispersion, absorption of the prepared films and the effects of light on the electrical characteristics of the prepared heterojunction are also considered to investigate the photodiodes applications.

2. Experimental

2.1. Preparation of the ligand

Synthesis of 5, 6 diphenyl-3-hydrazino-1, 2, 4-triazine (3-DHT) was prepared by a procedure reported in the literature [25]. A

* Corresponding author. Physics Department, Faculty of Science and Arts, Aljouf University, Saudi Arabia.

http://dx.doi.org/10.1016/j.molstruc.2017.03.020
0022-2860/

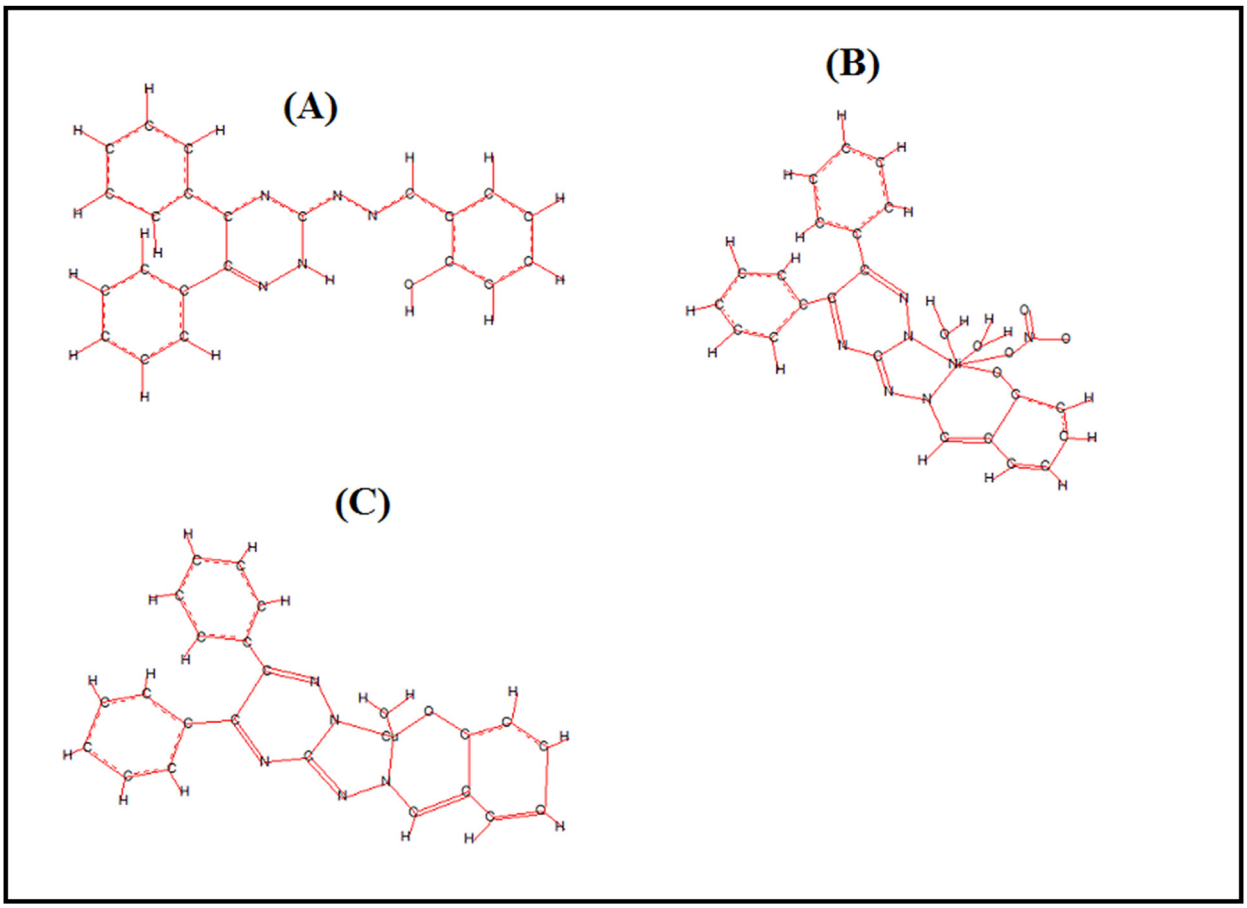

Fig. 1. Scheme of the proposed structures of (a) HBDHT compound,(b) Ni complex and (c) Cu complex.

mixture of ***3-DHT*** (5.26 g, 20 mmol) and salycyaldehyde (4.20 g, 20 mmol) in 50 mL ethanol was heated under reflux for 30 min. Yellow crystals were obtained after cooling at room temperature. The product was filtered off and recrystallized from aqueous ethanol (1:3), yield 5.15 g (72%) and m.p. 267 °C of the corresponding Schiff base 2-benzylidene-3-hydroxy-1-(5, 6-diphenyl-1, 2, 4-triazine-3-yl) hydrazine (HBDHT), (Fig. 1A).

2.2. Synthesis of the metal complexes

To a stirred ethanolic solution of an appropriate Ni(II) or Cu(II)-nitrate (0.01 mol, ~20 ml), an ethanolic solution of HBHDT (3.67 g, 0.01 mol, in 25 mL) was added in the molar ratio 1:1. The reaction mixture was stirred for 1 h at room temperature. The resulting brown precipitate was filtered off, washed with ethanol and diethyl ether and stored in desiccator on anhydrous calcium chloride. The analytical chemical composition and some physical properties are depicted in Table 1 and shown in Fig. 1.

2.3. Materials and methods

All chemicals used were of reagent grade. IR spectra were recorded with the FT-IR–8101 Shimadzu spectrometer (4000-400 cm^{-1}) as KBr pellets. FT Far-IR spectra have been recorded with a Nicolet 20F Far-IR vacuum spectrometer (FTIR) with a TGS (room temperature) detector using polyethylene wafers. Electronic absorption spectra were measured in methanol solution using a Perkin-Elmer 550 S spectrophotometer. Magnetic moments were obtained using the MSB-AUTO magnetic susceptibility balance by the Gouy method.

Thin films of Ni(II) complex were prepared by spin-coating technique, type Polos. The films were studied by using scanning electron microscope (SEM) of type JEOL-JSM-636 OLA. Photoluminescence characteristics were measured using RF-5301. Optical transmission and reflection were measured by using double beams spectrophotometer type JASCO – 670 of spectral range 200–2500 nm with a step scan of 2 nm. Single crystalline of p-type

Table 1
Analytical and physical data of HBDHT and its metal complexes.

No	Complex/empirical formula	FW	color	M.P	Analytical, calc (found)			Λ (ohm^{-1} cm^2 mol^{-1})	μ_{eff} (BM)
					C%	H%	N%		
1	HBDHT $C_{22}H_{17}N_5O$	367	yellow	267 °C	70.20 (71.94)	4.80 (4.63)	18.00 (19.00)	–	–
2	$[Ni(BDHT)(NO_3)(H_2O)_2)]\cdot H_2O$ $C_{22}H_{20}N_6O_7Ni$	540	Brown	215 °C	48.83 (48.89)	4.10 (4.11)	15.53 (14.80)	35	1.56
3	$[Cu(BDHT)(H_2O)](NO_3)\cdot H_2O$ $C_{22}H_{20}N_6O_6Cu$	527.5	brown	282 °C	50.05 (50.14)	3.82 (3.83)	15.92 (15.95)	44	1.96

Table 2
IR and far –IR spectroscopy of HBDHT and its metal complexes.

HBDHT	[Cu(BDHT)(H_2O)](NO_3)·H_2O	[Ni(BDHT)(NO_3)($H_2O)_2$)]·H_2O	Assignment
	IR- spectra		
3700-3200b	3410b	3412b	νOH/H_2O
3312S	3300S	–	ν(NH)
1620S	1605S	1601S	ν(C=N)
1510s	1513s	1512S	ν(C=C)
_	1383 S, 839 S	1369S, 833s	ν(NO_3)
1246 m	1233 m	1242 s	ν(C–O) phenolic
	Far-IR bands		
545,390,296,270	551, 361, 274	542,365,271	ν(triazine ring)
_	476, 275	475, 272	ν(M – N)
_	440, 397	438, 390	ν(M – O)

Si (100) wafers with the carrier concentration of $10^{16}cm^{-3}$ were purchased from Nippon Mining Co. and etched by using the CP4 solution (HF:HNO_3:CH_3COOH with ratio 1:6:1). The current–voltage characteristics of the heterojunction were measured by means of high impedance electrometer type Keithley 2635 A attached with a personal computer interfaced via certain proper software for recording and plotting the extracted data from the electrometer. Illumination of the hetero-junction was achieved by using a white halogen-tungsten with intensity measured using a solar power meter type TM-206.

3. Results and discussion

3.1. Spectral characterization

The prepared metal complexes are all air-stable solids and have good stoichiometry. The FT-IR data of the current ligand and its complexes are listed in Table 2 and shown in Fig. 2. The FT-IR spectra of the free ligand exhibit the characteristic bands of phenolic OH and NH stretching vibration groups (3700-3200 cm^{-1}), the high broadness might arise from the strong hydrogen bond and/or overlap with NH stretching vibration. In addition, two bands at 1620 and 1510 cm^{-1} were assigned to (C=N) and C=C groups as shown in Fig. 2. Similar features are observed in the IR spectra of the complexes, with the C=N stretching vibrations are shifted to lower wave numbers with respect to the free ligand appearing at (1605 and 1601 cm^{-1}) for Cu(II) and Ni(II)-complexes, indicating the participation of the C=N group in complexation. This fact is further supported by the appearance of medium intensity band in the region below 475 cm^{-1} that assignable to ν(M – N) vibration. Furthermore, the negative slope of the linear correlation of $\nu_{C=N}$ versus the calculated dipole moment (μ), μ/BM = 508–0.313 $\nu_{C=N}/cm^{-1}$, r = 0.92, F = 11.46, reveals a red shift of ν C=N (strong coordination) was accompanied by increasing the dipole moment of the complex.

On the other hand, the broad band in the range of 3700–3200 cm^{-1} in the free ligand HBHDT disappeared or displayed a red shift to 3410 cm^{-1} which might attribute to coordinated of water or phenolic OH group. This emphasized by the appearance of one more medium intensity band at 440 cm^{-1} assignable to ν (M – O) vibration. In the complexes, new bands observed at ca. 1369, 1383 cm^{-1} (ν_3) and 833, 839 cm^{-1} (ν_2) for Ni(II)- and Cu(II)-complexes, respectively, are consistent with the mono-dentate nature of the nitrate group [26,27]. This interpretation emphasized by the low conductance values: 33 and 44 $^{-1}$ cm^2 mol^{-1} listed in Table 1, for the current Ni(II)- and Cu(II)-complexes. Thus, from the IR-spectral assignments it is clear that the ligand behaves as tridentate towards the metal ion through the imine nitrogens and phenolic oxygen.

3.2. Electronic spectra characterization

The UV–visible spectra of the ligand and its complexes were recorded in methanol solution in the 200–800 nm region. The absorption spectra of HBHDT ligand consists of an intense band centered at 333 nm, attributing to n → π^* transitions. Furthermore, two intense bands at 303 and 213 nm for HBDHT were related to π → π^* transitions of aromatic rings and the azomethine groups. These transitions are also found in the spectra of the complexes, but they shifted toward lower frequencies, confirming the coordination of the ligand to the metal ion. The UV–visible spectra of the Ni(II) complex shows three absorption bands, 409,308, 219 nm and 403, 306, 250 nm for Cu(II)-complex, respectively [28–31].

3.3. Absorption and emission properties

To gain insight of the optical property and electronic transition, the excitation energy and UV–Vis absorption spectra for the

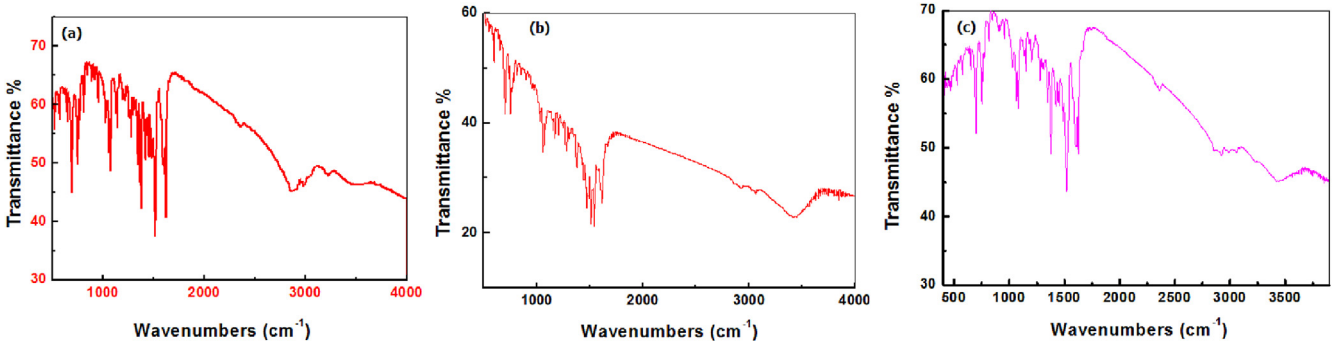

Fig. 2. FT- IR Spectrum of (a) HBDHT compound,(b) Ni complex and (c) Cu complex.

Table 3
Excitation wave length, emission bands and λ_{scot} of HBDHT ligand and its metal complexes in methanol solvent.

Compound	λ_{max} (nm)	λ_{ex} (nm)	λ_{em} (nm)	λ_{scot} (nm)
HBDHT ligand	333- 303-213	260	503 (7×10^6)[a]	243
[Ni(BDHT)(NO_3)($H_2O)_2$)]·H_2O	409-308-219	300	390 (5.8×10^6)[a]	90
[Cu(BDHT)(H_2O)](NO_3)·H_2O	403-306-250	260	380 (6×10^6)[a]	120

[a] Molar absorptivity (ε).

Table 4
Structural parameters of HBDHT ligand and its metal complexes computed by means of DFT using the B3LYP and the basis set 6-31G level, provides by the Gaussian 09 program.

Compound	E_{tot} (eV)	Dipole Moment μ/D	ΔHf (eV)	E_{HOMO}(eV)	E_{LUMO}(eV)	E_{gap} (eV)
HBDHT ligand	−32573	0.6351	−25.15	−6.324	−0.033	6.286
$[Ni(BDHT)(NO_3)(H_2O)_2)]\cdot H_2O$	−77960	5.996	−39.59	- 6.503	0.052	6.555
$[Cu(BDT)(H_2O)](NO_3)\cdot H_2O$	−81255	6.559	−40.33	−6.340	0.076	6.264

singlet-singlet transition of all compounds were measured in methanol solution the band maxima are depicted in Table 3. The current compounds exhibit a strong absorption band in the UV region around 300 nm for free ligand and its complexes, which can be assigned to an intramolecular charge transfer (ICT) between the various donating unit and the electron acceptor, hydrogen bond acceptor and/or metal ion.

The measured wavelength λ_{abs} of the studied compounds decreases in the following order Ni(II)- complex > Cu(II)-complex ≫ HBDHT which is the same order of the band gap. This bathochromic effect from the free ligand (HBDHT) to metal ion is obviously due to increased π delocalization. This interesting point is seen both by analyzing electronic and absorption results. Excitation to the S1 state corresponds exclusively to the promotion of an electron from the HOMO to the LUMO. The absorption wavelengths arising from S0→S1 electronic transition increase progressively with the increasing of conjugation lengths.

In order to study the emission photoluminescence properties of the studied compounds, the adiabatic emission spectra were measured at room temperature in methanol. The emission spectral data of the compounds recorded in methanol are collected in Table 3. According to the absorption and emission data, the values of Stokes shift (SS) for all compounds were obtained. The emission spectra arising from S1 state is assigned to $\pi^* \rightarrow \pi$ and LUMO→HOMO transition character for all molecules. Through analyzing the transition configuration of the fluorescence, we found that the calculated fluorescence is just the reverse process of the lowest lying absorption. Moreover, the observed red-shifted emission of the photoluminescence (PL) spectra in order Cu (II)-complex < Ni (II)-complex ≪ HBDHT when passing from HBDHT to Cu (II)-complex ~ Ni (II)-complex is in reasonable agreement with the obtained results of absorption. Furthermore, the Stokes shift of these compounds is found to be in the range 90, 120 and 243 nm. These promising optical properties suggest that the current compounds will be good candidates for the solar cell devices.

3.4. Molecular orbital calculations

All molecular calculations were performed in the gas phase by means of Density Functional Theory (DFT) using the B3LYP and the basis set 6-31G level, provides by the Gaussian 09 program. The structural parameters data of the free ligand HBDHT and its metal complexes were calculated and listed in Table 4. In addition, the optimized structure of HBDHT and its metal complexes are shown in Fig. 3(a–c).

The frontier molecular orbital (FMO) contribution is very important in determining the charge-separated states of the studied molecules because the relative ordering of occupied and virtual orbital provides a reasonable qualitative indication of excitation properties and provides also the ability of electron hole transport [32,33]. The energies of the frontier molecular orbitals of studied molecules are given in Table 5. It is well known that the HOMO and LUMO energies and energy gaps are weightily relative to optical and electronic properties. Table 5 shows detailed data of absolute energy of the frontier orbital calculated by DFT for the studied molecules. The distributions and energy levels of the

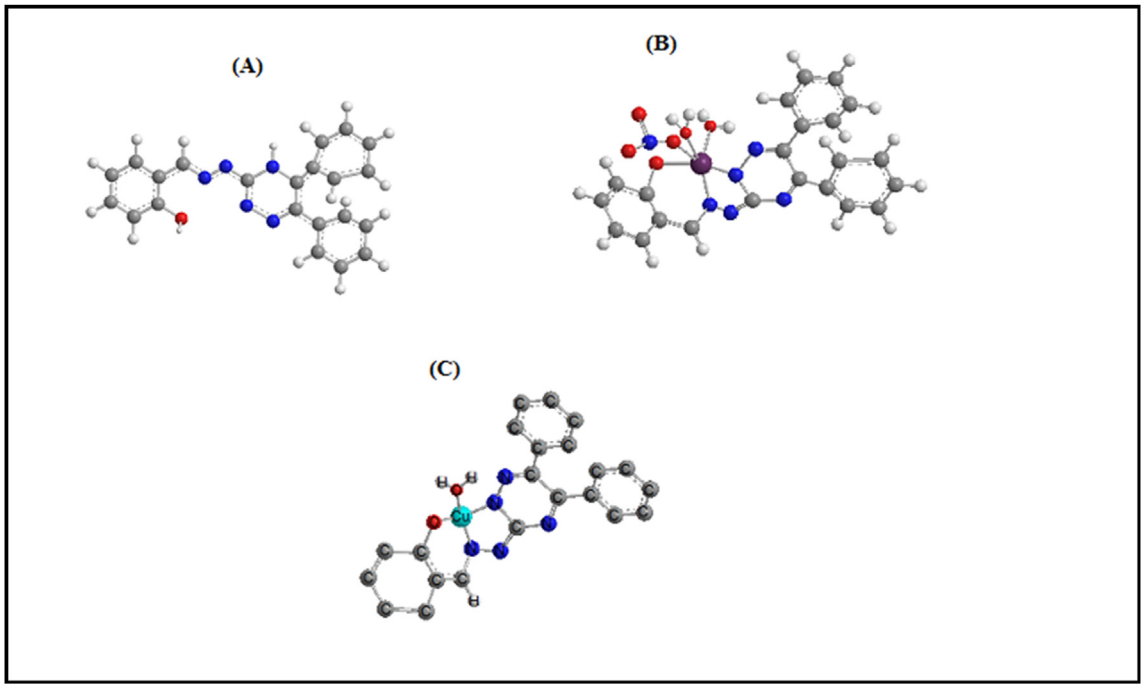

Fig. 3. (a) Optimized structure of HBDHT free lig. (b) Ni(BDHT) Complex, and (c) Optimized structure of Cu(BDHT) complex.

Table 5
Frontier orbitals data obtained by DFT method for the current compounds at B3LYP/6-31G optimized geometries.

Compounds	HOMO	HOMO-1	HOMO-2	LUMO	LUMO+1	LUMO+2	λ_{abs} (nm)	Electronic transitions	MO/character
HBDHT	−6.324	−6.890	−7.102	−0.0326	−0.0027	−0.0025	197.07	S 0 →S1	HOMO →LUMO
							180.80	S 0→ S2	HOMO-1→ LUMO
							175.38	S 0→ S3	HOMO-2→ LUMO
							196.14	S0 →S4	HOMO→ LUMO+1
							196.14	S0 →S5	HOMO→ LUMO+2
							180.01	S0→ S6	HOMO-1→ LUMO+1
Ni-complex	−6.503	−6.748	−6.892	0.0517	0.0598	0.0707	189.16	S 0 →S1	HOMO →LUMO
							182.35	S 0→ S2	HOMO-1→ LUMO
							178.75	S 0→ S3	HOMO-2→ LUMO
							188.94	S0 →S4	HOMO→ LUMO+1
							188.62	S0 →S5	HOMO→ LUMO+2
							182.14	S0→ S6	HOMO-1→ LUMO+1
Cu-complex	−6.340	−6.960	−7.271	0.0761	0.0431	0.0680	193.23	S 0 →S1	HOMO →LUMO
							176.21	S 0→ S2	HOMO-1→ LUMO
							168.75	S 0→ S3	HOMO-2→ LUMO
							194.23	S0 →S4	HOMO→ LUMO+1
							193.47	S0 →S5	HOMO→ LUMO+2
							177.04	S0→ S6	HOMO-1→ LUMO+1

HOMO-2, HOMO-1, HOMO, LUMO, LUMO+1 and LUMO+2 orbitals were computed at the B3LYP/6-31G level for the current compounds. Both the highest occupied molecular orbitals (HOMOs) and the lowest-lying unoccupied molecular orbitals (LUMOs) are mainly localized on the rings as shown in Fig. 4, indicating that the HOMO are mostly the π-antibonding type orbitals. The HOMO orbitals are mainly delocalized on the triazine group, while the LUMO orbitals are mainly delocalized on triazine group and phenyl rings. Namely, electron transitions are corresponding to the n-π^* and π - π^* electron transitions. The value of the energy separation between the HOMO and LUMO is 6.286 eV for the free ligand (HBDHT) and this low energy gap indicates that the current ligand is potentially interesting electronic transitions. However, the complexes of HBDHT show the following E_{HOMO} = −6.503, −6.340eV and E_{gap} = 6.555 and 6.264 eV for Ni(II)- and Cu(II)-complexes, respectively.

The HOMO and the LUMO energy levels of the donor and acceptor components are very important factors to determine whether effective charge transfer will happen between donor and acceptor. To evaluate the possibilities of electron transfer from the excited studied molecules to the conductive band of the acceptor TiO_2 or PCBM, the HOMO and LUMO levels were compared (Fig. 5). It is important to note that the LUMO levels of the current compounds are higher than that of the conduction band of TiO_2 (−4.0 eV) [34], and of PCBM (−3.7 eV) [35]. The HOMO energy levels of all dyes are much lower than that of both TiO_2 conduction band edge and PCBM suggesting that the photo-excited electron transfer from π to TiO_2 (or to PCBM) may be sufficiently efficient to be useful in photovoltaic devices.

The power conversion efficiency (ξ) was calculated according to the following Eq. (1):

$$\xi = \frac{FF\ V_{oc} J_{sc}}{P_{in}} \tag{1}$$

where P_{in}. is the incident power density, J_{sc} is the short-circuit current, V_{oc} is the open-circuit voltage, and *FF* denotes the fill factor.

The maximum open circuit voltage (V_{oc}) of the bulk heterojunction (BHJ) solar cell is related to the energy difference between the highest occupied molecular orbital (E_{HOMO}) of the electron donor and the lower unoccupied molecular orbital (ELUMO) of the electron acceptor, taking into account the energy lost during the photo-charge generation [35,36]. The theoretical values of open-circuit voltage Voc have been calculated from the following expression (2):

$$V_{oc} = |E_{HOMO}(\text{Donor})| - |E_{LOMO}(\text{Acceptor})| - 0.3 \tag{2}$$

The V_{oc} of the current compounds can be approximately estimated by the energy difference between E_{LUMO} of the investigated compound and conduction band (E_{CB}) of the semiconductor [37]:

$$V_{oc} = E_{LUMO} - E_{CB} \tag{3}$$

As shown in Table 6, the theoretical values of the open circuit voltage V_{oc} of the studied molecules range from 3.867 eV to 4.076 eV of TiO_2 (2.503−2.890 eV of PCBM). These values are sufficient for a possible efficient electron injection. Therefore, all the studied molecules can be used as sensitizers because the electron injection process from the excited molecule to the conduction band of the acceptor (TiO_2) is possible and can also be used as organic molecules in solar cells with the presence of acceptor sites.

3.5. Morphology characterization

Surface morphology characterization of **Ni(BDHT)** thin films was achieved by using scanning electron microscope (SEM) with different magnifications as shown in Fig. 6(a)-(d). This figure demonstrates a high crystalline growth of the film on the substrate. The overall characteristics of the presented images appear well crystalline thin films with randomly oriented distribution and different sizes and orientations as well as aggregation. It is difficult to estimate the particle size by using the SEM images due to the presence of large and fine particles with a heterogeneous distribution of particles with various morphologies; therefore the particle size analyzer was used. The distribution of the particle size is shown in Fig. 7 which shows the predominant size is found to ~300 nm. The obtained results support the applicability of the grown films with high crystallinity and particle size for optoelectronics as suggested by Werner and Bermann [38]. They discussed the enhancement of the open circuit voltage and other solar cell parameters for the films of sizes within the range of 100 nm-10 μm. Yamamoto and Romeo et al. [39] have studied the referred this relationship to the influence of lower grain boundaries [40]. Wang et al. [41] have reported that the nanoparticles with various sizes are preferred to have various absorption edges due to the influence of quantum confinement. Mastroianni et al. [42] have suggested that the small size of the grown crystals originate a great number of grain boundaries and crystal dislocations that affect the solar

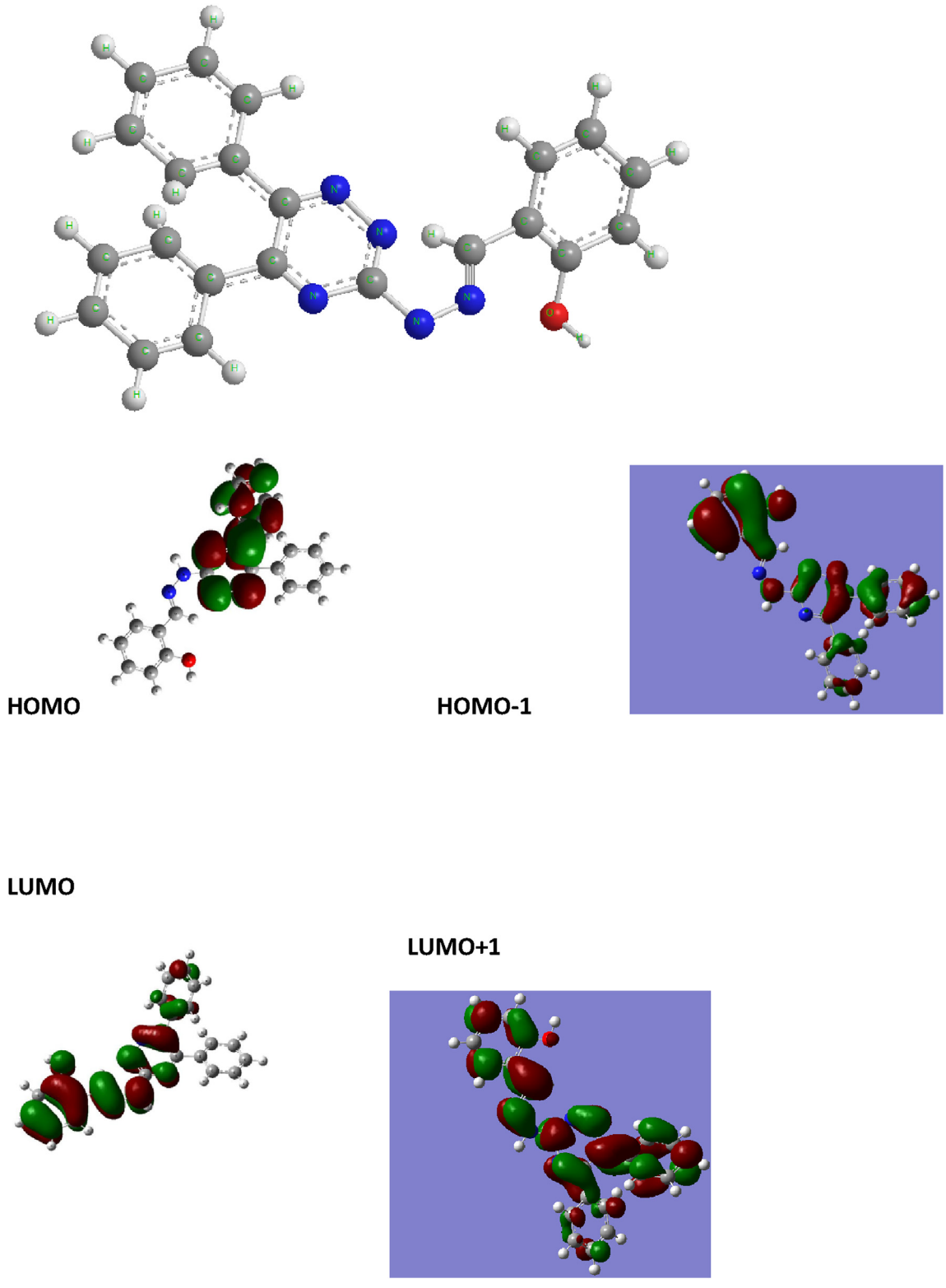

Fig. 4. The contour plots of HOMO's and LUMO′ orbitals of HBDHT compound.

device efficiently.

3.6. Optical characterization

Spectral dependence of transmittance T(λ) and reflectance R(λ) of the Ni(BDHT) thin films over wavelength range of 200–2500 nm are shown in Fig. 8. It is clear from the figure that a remarkable transmission edge is detected which confirming this film as a probable optical filter. Furthermore, the spectral distribution at longer wavelengths (λ > 900 nm), the film becomes transparent

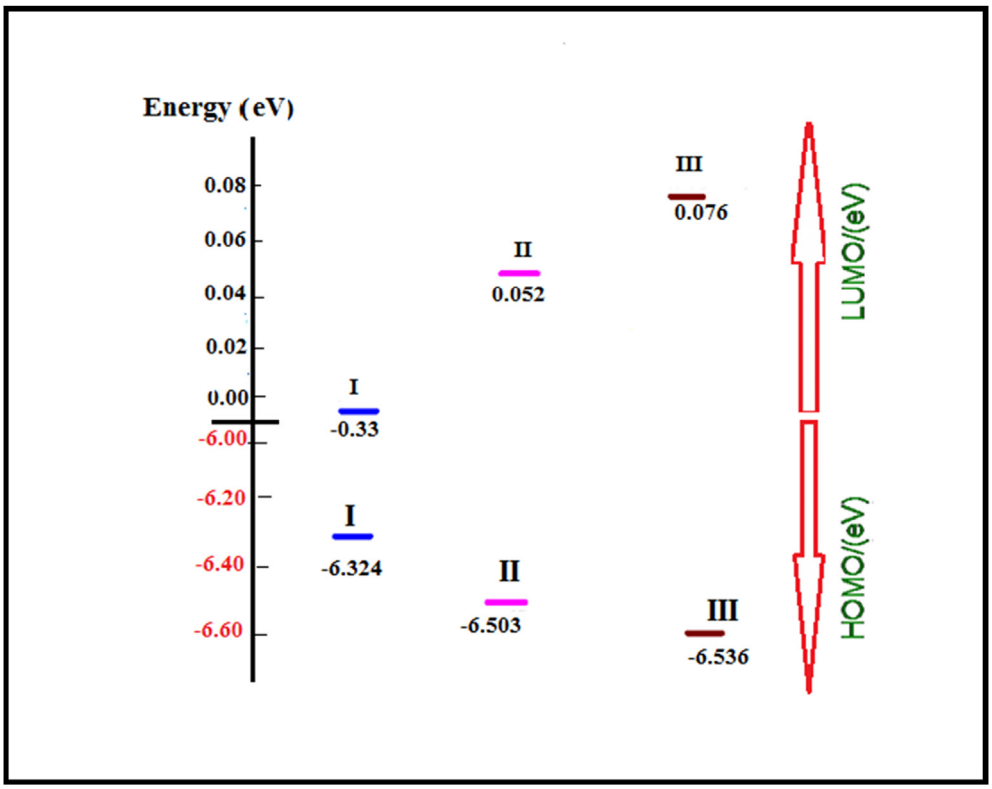

Fig. 5. Sketch of B3LYP/6-31G calculated energies of the HOMO, LUMO level of studied molecules I= HBDHT,II= Ni(II)complex and III= Cu(II)Complex.

Table 6
Energy values of LUMO(E_{LUMO}), HOMO (E_{HOMO}) and the open circuit voltage V_{oc} of the studied molecules obtained by B3LYP/6-31G level.

Compound	E_{HOMO}(eV)	E_{LUMO}(eV)	V_{oc}/absolute (eV)	V_{oc}/TiO_2(eV)[a]	V_{oc}/PCBM(eV)[a]
HBDHT	−6.890	−0.0327	6.557	3.967	2.890
Ni(II)-complex	−6.503	0.0517	6.151	4.052	2.503
Cu(II)-complex	−6.536	0.0762	6.160	4.076	2.536

[a] TiO_2 -4.0 eV and PCBM -3.7 taken from ref. [37].

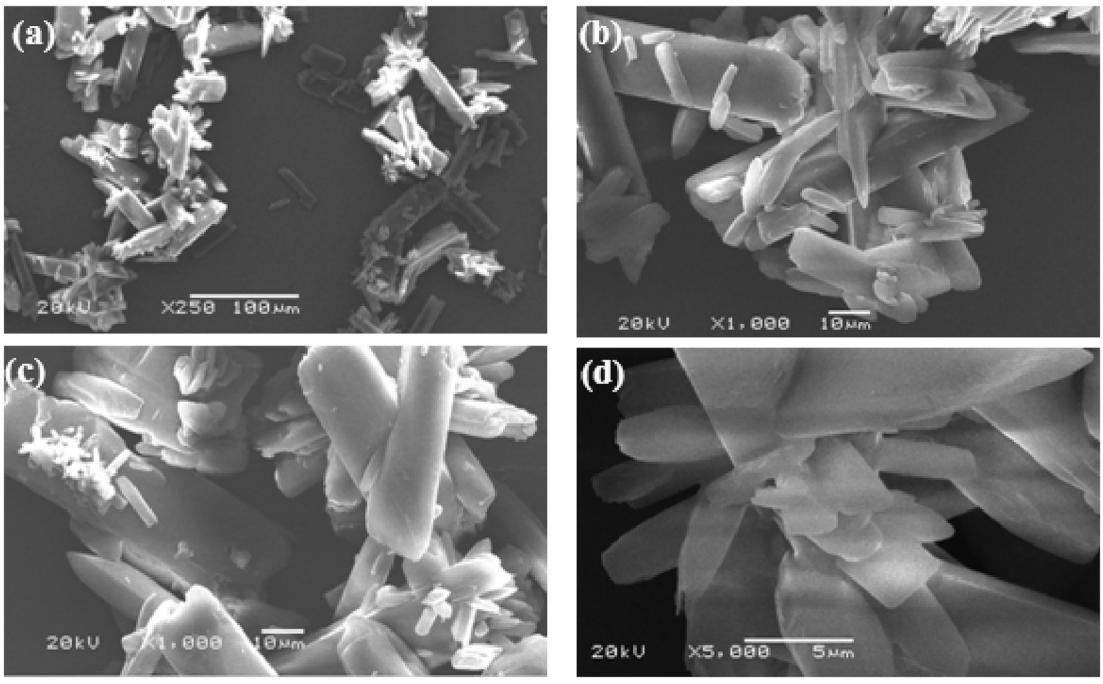

Fig. 6. SEM image of different magnifications (a) 250× and (b) 1000×, (c) 1000× with zoom −in, and (d) 5000× of $[Ni(BDHT)(NO_3)(H_2O)_2)]\cdot H_2O$ thin films.

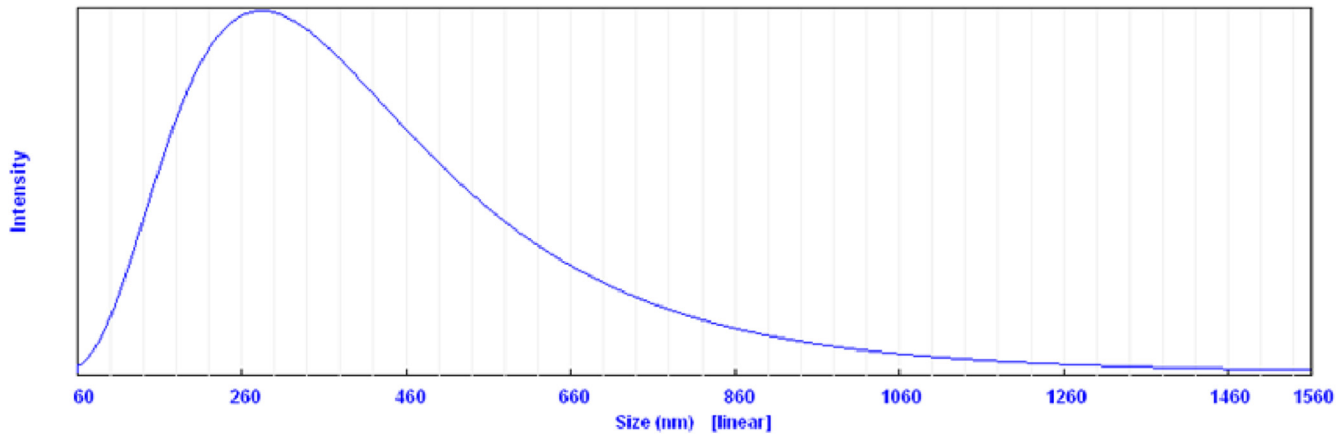

Fig. 7. Particle size distribution of $[Ni(BDHT)(NO_3)(H_2O)_2)]\cdot H_2O$.

appearing that there is no light is absorbed without any scattering or absorption (i.e. ~R + T = l). However, in the absorption region gaps were estimated by employing Bardeen's formula as follows [43–45]:

$$(\alpha h\nu) = A(h\nu - E_g)^s, \quad (4)$$

where A is a constant related to prospect of transition, s is an exponent defines the transition type, which have a value of 1/2 and 3/2 for the direct allowed and direct forbidden transitions, respectively. While, s = 2 and 3 for indirect allowed and indirect forbidden transitions, respectively [46].

The above formula was used with all the probabilities of transition and the best fit was set for $s = 1/2$, which means the predominant of transition with a type of indirect allowed. Plot of $(\alpha h\nu)^{1/2}$ vs. $h\nu$ for the Ni(BDHT) thin films is shown in Fig. 9(a) and (b). As observed, the energy band gap can be obtained from a straight line extrapolation with the photon energy axis at $(\alpha h\nu)^{1/2} = 0$ gives the optical band gap. Two extracted optical gaps E_{g1} and E_{g2} with values of 1.1 and 2.55 eV, respectively. The obtained values of energy gaps are found to be in agreement with other organic films [47–52], and confirm that the presented structure is anticipated to be preferable for photovoltaic applications [53]. The estimated energy gap is determined by the calculations based on molecular orbital which explained on the bases of single molecule in its calculation (in the light of Van der Waals of solids) [54].

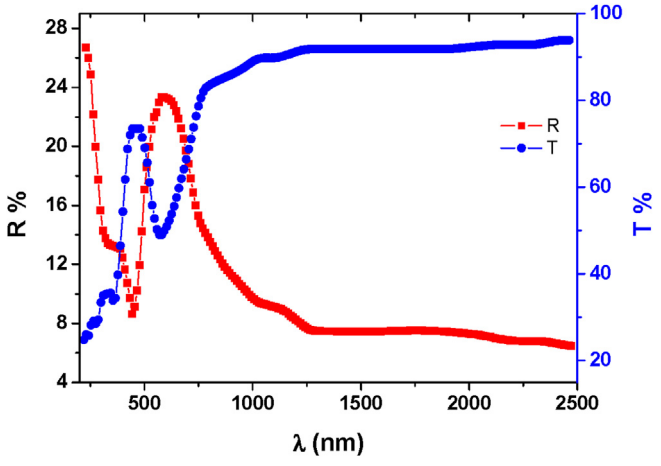

Fig. 8. Spectral behavior of the transmittance T(λ) and the reflectance R(λ) of $[Ni(BDHT)(NO_3)(H_2O)_2)]\cdot H_2O$ thin films.

3.7. Dielectric characterizations

Dielectric dispersion of the dielectric constant has a potential interesting for characterizing the prevalence of the electromagnetic waves and the light loss in the solid material, suitable for optoelectronic application [55]. The complex dielectric constant, related to the real dielectric, ε_1 constant and the imaginary dielectric constant, ε_2, can be described by the following formula [55].

$$\varepsilon = \varepsilon_1 - i\varepsilon_2 \quad (5)$$

And the loss factor can be specified by the following equation

$$\tan\delta = \frac{\varepsilon_1}{\varepsilon_2} \quad (6)$$

The photon energy dependence of ε_1 and ε_2 is illustrated in Fig. 10. As observed, the same tendency of ε_1 and ε_2 occurs. In addition, the loss factor, tanδ, of the Ni (BDHT) thin films has been determined by the above equation and the photon energy dependence is shown in Fig. 11. In addition, the photon energy dependence of the real, σ_1 and imaginary, σ_2 parts of the optical conductivity are shown in Fig. 12. As observed from the figure that the two parts of the optical conductivity have the same trend. The photon energy dependence of the latter parameters may be due to some changes in the structure of the film as discussed before in the literature by various authors [55–57].

3.8. Current density–voltage characteristics

Semi-logarithmic plot of forward and reverse bias J–V characteristics of Ni(HBDHT)/p-Si is illustrated Fig. 13 in dark and under various illuminations of 40–100 mW/cm^2 at 300 K. A remarkable rectification behaviour is detected, supporting the formation of barrier at Ni(HBDHT)/Si interface. In addition, the rectification ratio (RR) is found to decrease with increasing illumination intensity as shown in Fig. 14 (a) which confirms the behaviour of photodiode [58]. The J–V characteristics can be described by the following relation for a limit region ($V_F \geq 3$ kT/q) [59,60]:

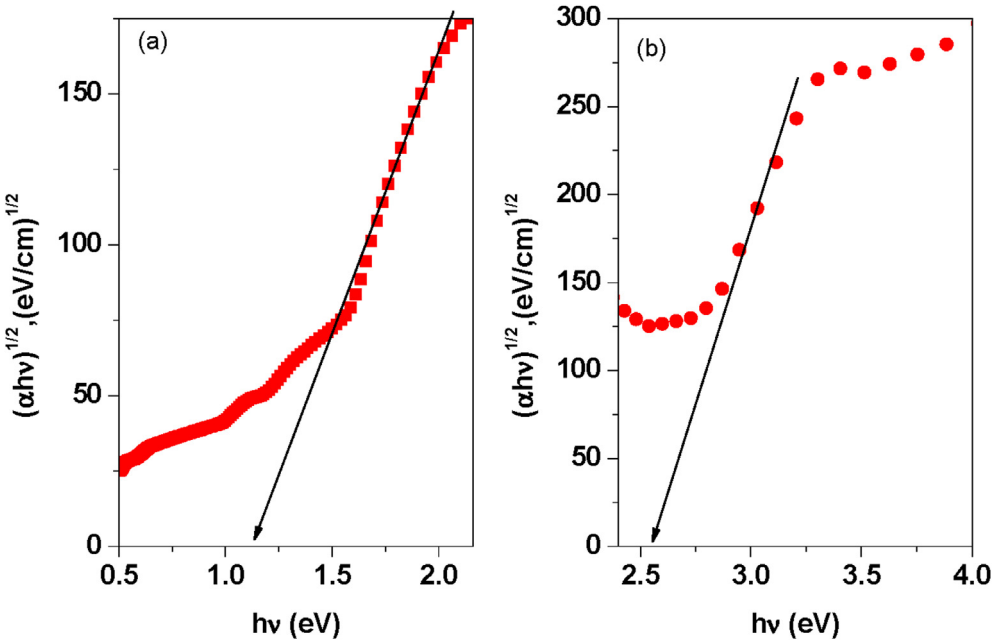

Fig. 9. Plot of $(\alpha h\nu)^{1/2}$ vs. hν (a) first region and (b) second region of $[Ni(BDHT)(NO_3)(H_2O)_2)]\cdot H_2O$ thin films.

$$J = J_0\left[\exp\left(\frac{q(V - JR_s)}{\eta kT}\right) - 1\right] \tag{7}$$

where V is the applied voltage, η is the ideality factor, k is the Boltzmann constant, T is the absolute temperature, R_s is the series resistance and the reverse saturation current density J_o is defined by the following:

$$J_0 = A^* T^2 \exp\left(\frac{-q\Phi_b}{kT}\right) \tag{8}$$

where, A^* is the Richardson constant and Φ_b is the zero-bias barrier height which can be estimated from the y-axis intercept using the following relation:

$$\Phi_b = \frac{kT}{q}\ln\left(\frac{A^* T^2}{J_0}\right) \tag{9}$$

Furthermore, the ideality factor, η can be estimated from the slope of *J-V* characteristics using the following equation

$$\eta = \frac{q}{kT}\left(\frac{dV}{d\ln(J)}\right) \tag{10}$$

In addition, the photocurrent as function of light intensity is shown in Fig. 14 (b). As observed, an increase in the photocurrent with increasing light intensity. Accordingly, this gives an indication for the production of an excitation as a result of light absorption and the dissociation of this excitation at the organic/inorganic interface by the effect of internal electric field. Therefore, the photocurrent increases with increasing the light intensity according to the well-known equation ($I_{ph} = CP^{\gamma}$, where I_{ph} is the photocurrent, C is a constant, γ is an exponent, and P is the illumination intensity [61].

The slope of the linear fitting of logarithmic plot of *I-P* characteristic (Fig. 14(b)) is found to be ~0.9 which confirms a prospect of trap centres occurrence through the band gap as discussed by Soylu

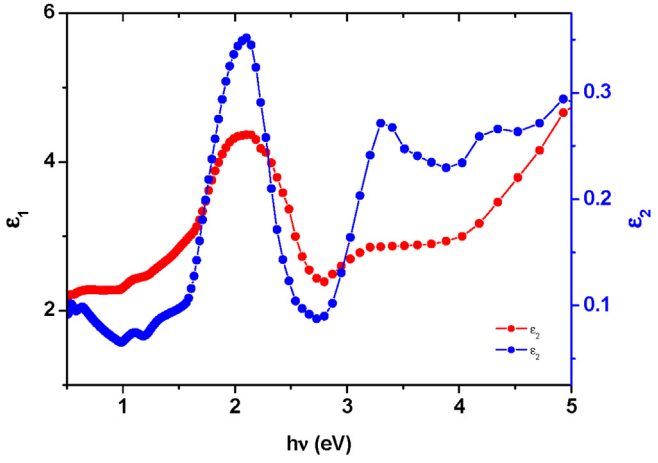

Fig. 10. Photon energy dependence of ε_1 and ε_2 of $[Ni(BDHT)(NO_3)(H_2O)_2)]\cdot H_2O$ thin films.

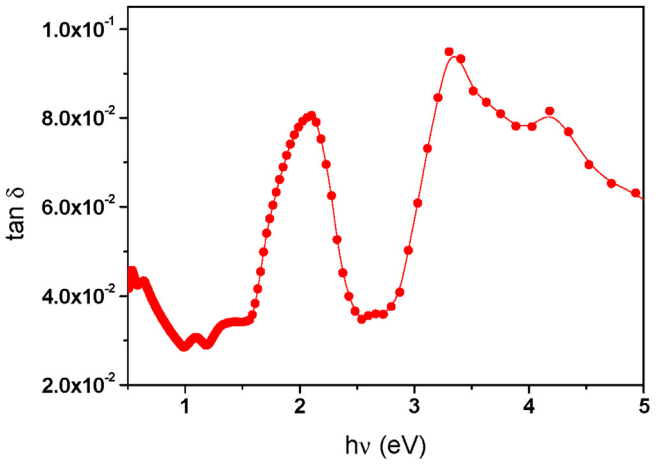

Fig. 11. Photon energy dependence of tan δ of $[Ni(BDHT)(NO_3)(H_2O)_2)]\cdot H_2O$ thin films.

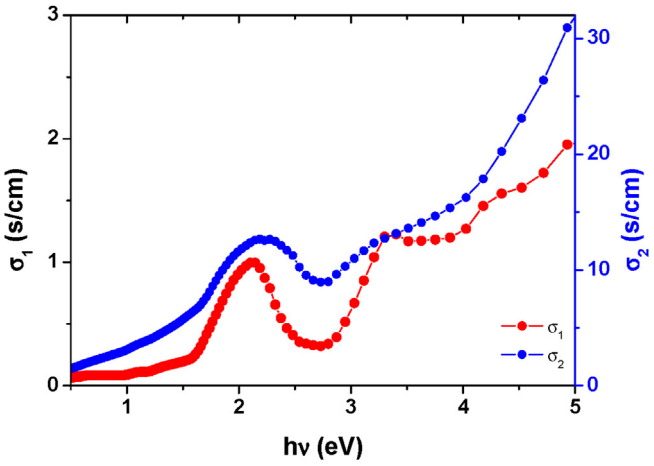

Fig. 12. Photon energy dependence of σ_1 and σ_2 of $[Ni(BDHT)(NO_3)(H_2O)_2)]\cdot H_2O$ thin films.

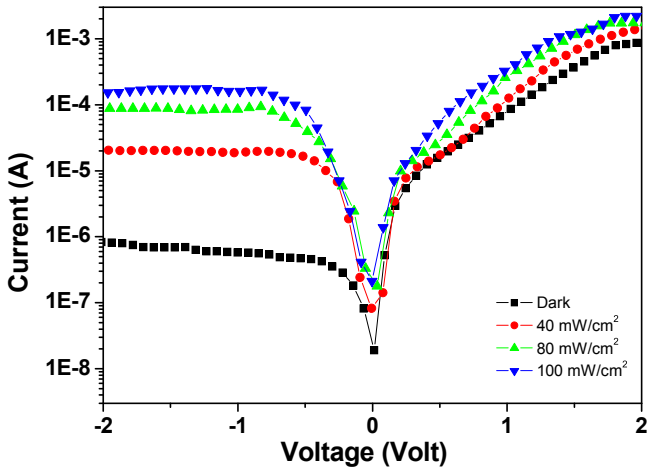

Fig. 13. Plot of current -voltage characteristics of $[Ni(BDHT)(NO_3)(H_2O)_2)]\cdot H_2O$/p-Si heterojunction.

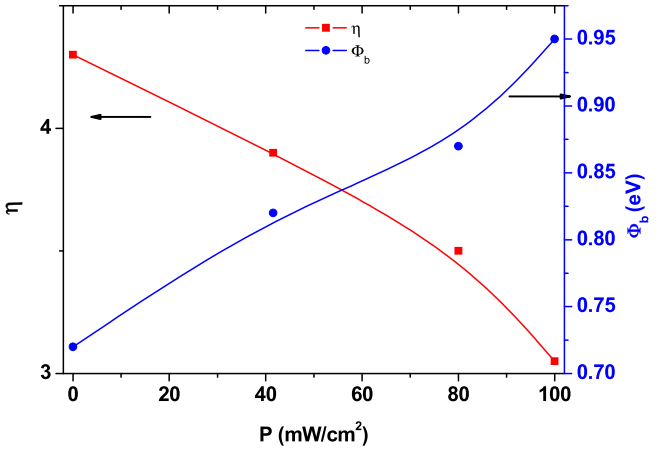

Fig. 15. Plot of η vs. P and Φ_b vs. Voltage of $[Ni(BDHT)(NO_3)(H_2O)_2)]\cdot H_2O$/p-Si heterojunction.

et al. [62]. Therefore, the generation procedure for the photocurrent can powerful be influenced by the located traps [62].

Values of Φ_b of the diode were calculated by sing the intercept of Fig. 15 and Eq. (9). Variation of Φ_b as a function of illumination intensity is illustrated in Fig. 15. As observed, values of Φ_b is found to be increase with increasing light intensity which can be understood explained by the generation of additional carriers having enough energy to overcome the higher barriers [63].

The ideality factor was determined using the slope of Fig. 15 and Eq. (10). As observed in Fig. 15, the determined ideality factor is shifted from unity and found to decrease with increasing light intensity. Deviation from the standard diode case may be explained by charge carriers' recombination through the depletion region [64]. The enhancement for the ideality factor is taken place under effect of illumination intensity as observed from the decrease of ideality factor from 4.2 to 3.1. The corrected value for the barrier height can be obtained from the relationship of barrier height versus ideality factor at different light intensity, as shown in Fig. 16 (a). As observed, the corrected value of barrier height which corresponds to ideality factor ~1 equals 1.125 eV.

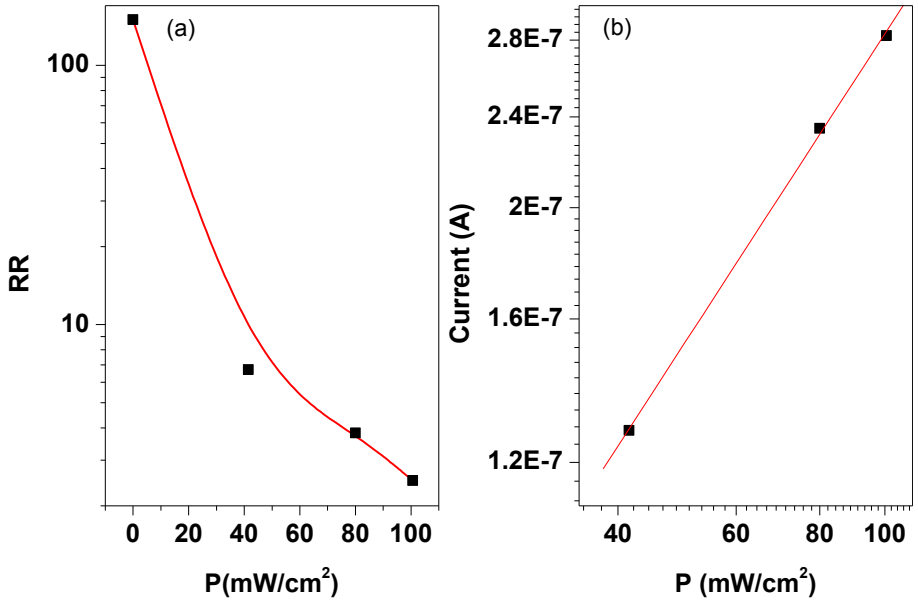

Fig. 14. (a) Plot of RR vs. P and (b) Logarithmic plot of current vs. P of $[Ni(BDHT)(NO_3)(H_2O)_2)]\cdot H_2O$/p-Si heterojunction.

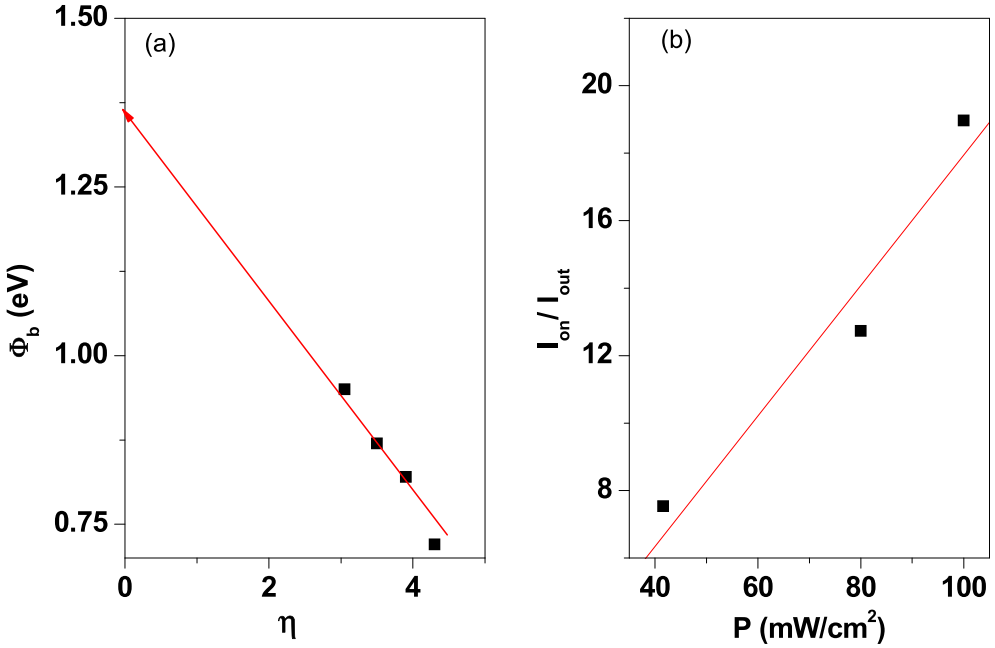

Fig. 16. (a) Plot of Φ_b vs. η and (b) Plot of I_{on}/I_{off} vs. P of $[Ni(BDHT)(NO_3)(H_2O)_2)]\cdot H_2O$ complex/p-Si heterojunction.

Study of ideality factor and the barrier height under different illumination intensity were studied elsewhere [65,66] and elucidated by the fact that the presence of barrier height inhomogenities of and/or the presence of interfacial layer at metal/semiconductor [66].

Ratio of J_{on} (i.e. current under illumination) to J_{off} (i.e. dark current) at a certain voltage is defined as photoresponsivity which is a characteristic for the photodiode. The ratio J_{on}/J_{off} as a function of light intensity is shown in Fig. 16(b). A remarkable photoresponsivity is demonstrated with a linear-fit characteristic. Accordingly, this result confirms the possibility for the prepared heterojunction for the application as a photodiode [67].

Fig. 17(a) shows the loaded current density-voltage characteristics of Ni(BDHT)/p-Si under different illumination intensities of the range 20–100 mW/cm^2 at 300 K. In addition, of the output power-voltage curve of the heterojunction is shown in Fig. 17(b). It can be seen from the figures that the photovoltaic parameters are small as compared with those for inorganic heterojunction and similar to most of the organic/inorganic heterojunctions. These figures give an indication for the degree of the excitons disassociation process [68] Furthermore, the obtained open-circuit voltage (i.e. 0.2 eV) is smaller than those obtained from the theoretical one by B3LYP/6-31G level. The contradiction between them can be attributed from the fact that most of the theoretical calculations

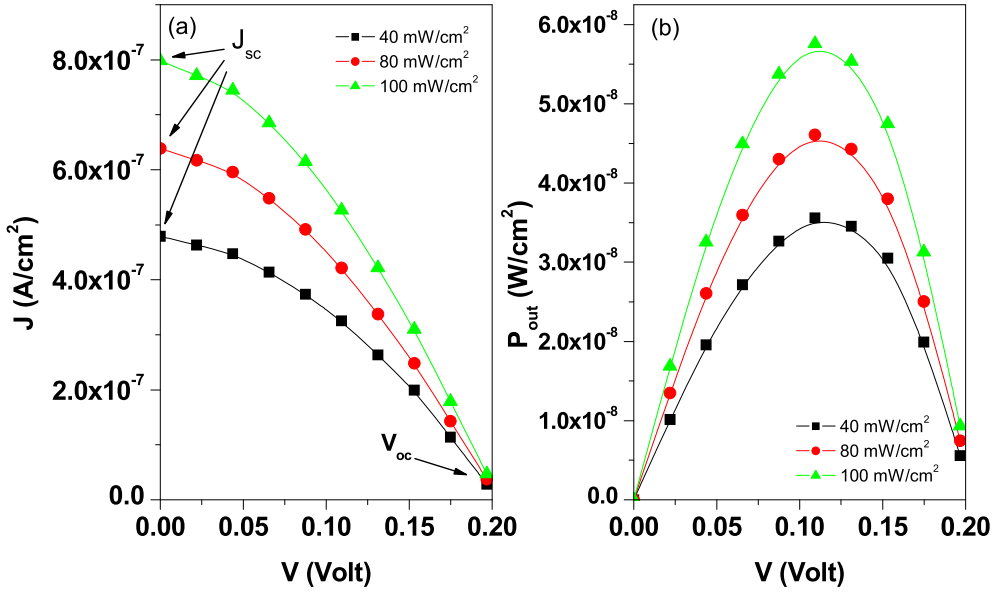

Fig. 17. (a) Plot of J vs. V and (b) Plot of P_{out} vs. V under different light intensities of $[Ni(BDHT)(NO_3)(H_2O)_2)]\cdot H_2O$ complex/p-Si heterojunction.

were carried out for models underlying considering infinitely dilute solutions [54].

4. Conclusions

The studied metal complexes were found that the ligand, HBDHT bonded to metal ions through the imine nitrogen and phenolic oxygen as confirmed by the IR-spectral assignments.

The lower value of the magnetic moment of Ni (II) complex can be due to the equilibrium between octahedral and square planar geometry.

The estimated particle size is found to be ~300 nm as detected from the distribution of the particle size analyzer. The obtained results confirms the availability of the grown films with high crystallinity and suitable particle size for optoelectronic applications. The results of the absorption spectra show three main characteristic bands which can be attributed to n-π^* transition (R-band) for the first and second but third band could be due to $\pi-\pi^*$ transitions over the whole conjugated system (K-band). Two optical gaps Eg_1 and Eg_2 with a values of 1.1 and 2.55 eV, respectively were characteristics for Ni(BDT) thin films.

Heterojunctions of Ni (BDHT)/p-Si show good rectifying characteristics and high photocurrent under a reverse bias as compared to forward one which confirms photodiode behavior. The extracted heterojunction parameters are found to be affected by illumination intensity in the range 40–100 mW/cm^2. A linear response of the photocurrent with light intensity on the logarithmic scale supports the high photosensitivity as well as the presence of continuous distribution of trap levels. The photovoltaic parameters were estimated and compared to study the applicability of the prepared heterojunction for optoelectronic device application.

References

[1] B.A. El-Shetary, M.S. Abdel-Moez, S. Abo El-Wafa, F.I. Zidan, H.S. Sleem, Thermochim. Acta 119 (1987) 249–259.
[2] F.A. Snavely, B.D. Krecker, C.G. Klark, J.Am. Chem. Soc. 79 (1957) 1028–1030.
[3] V.V. Dabholkar, O.G. Yadav, N.B. Shinde, A.M. Mohammed, Der Pharma Chem. 7 (2015) 95–99.
[4] P. Jayaroopa, G.V. Kumar, N. Renuka, M.A.H. Nayaka, K.A. Kumar, Int. J. Pharm. Tech. Res. 5 (2013) 264–270.
[5] M. Govindaraju, G.V. Kumar, G. Pavithra, M.A.H. Nayaka, B.N. Mylarappa, K.A. Kumar, IOSR J. Pharm. Biol. Sci. 2 (2012) 30–34.
[6] I. Yildirim, N. Ozdemir, Y. Akçamur, M. Dinçer, O. ndaç, Acta Cryst. E61((2005) 256–258.
[7] N.M. Abunada, H.M. Hassaneen, N.G. Kandile, O.A. Miqdad, Molecules 13 (2008) 1501–1517.
[8] M. Ezawa, D.S. Garvey, D.R. Janero, S.P. Khanapure, L.G. Letts, A. Martino, R.R. Ranatunge, D.J. Schwal, D.V. Young, Lett. Drug Des. Discov. 2 (2005) 40–43.
[9] H. Suleyman, E. Buyukokuroglu, M. Biol. Pharm. Bull. 24 (2001) 1133–1139.
[10] A.H. Abadi, A.A. Haleem Eissa, G.S. Hassan, Chem. Pharm. Bull. 51 (2003) 838–844.
[11] O. Pouralimardan, A.-C. Chamayou, C. Janiak, H. Hosseini Monfared, Inorg. Chim. Acta 360 (2007) 1599–1608.
[12] Z.J. Xu, R. Fang, C. Zhao, J.-S. Huang, G.-Y. Li, N. Zhu, C.M. Che, J. Am. Chem. Soc. 131 (2009) 4405–4417.
[13] K.P. Gosden, D. Pletcher Healy, J. Chem. Soc. Dalton Trans. (1978) 972–976.
[14] C.C. Kwok, S.C. Yu, I.H.T. Sham, C.M. Che, Chem. Commun. (2004) 2758–2759.
[15] A. Trujillo, M. Fuentealba, D. Carrillo, C. Manzur, I. LedouxRak, J.R. Hamon, J.Y. Saillard, Inorg. Chem. 49 (2010) 2750–2764.
[16] C.M. Che, S.C. Chan, H.F. Xiang, M.C.W. Chan, Y. Liub, Y. Wang, Chem. Commun. (2004) 1484–1485.
[17] J. Gradinaru, A. Forni, V. Druta, F. Tessore, S. Zecchin, S. Quici, N. Garbalau, Inorg. Chem. 46 (2007) 884–895.
[18] L. Wang, W. Qin, X. Tang, W. Dou, W. Liu, Q. Teng, X. Yao, Org. Biomol. Chem. 8 (2010) 3751–3757.
[19] J.C. Hindson, B. Ulgut, R.H. Friend, N.C. Greenham, B. Norder, A. Kotlewskic, T.J. Dingemans, J. Mater. Chem. 20 (2010) 937–944.
[20] M.L. Petrus, T. Bein, T.J. Dingemans, P. Docampo, J. Mater Chem. A 3 (2015) 12159–12162.
[21] D. Isik, C. Santato, S. Barik, W.G. Skene, Org. Electron 13 (2012) 3022–3031.
[22] J.L. Sicard, D. Navarathne, T. Skalski, W.G. Skene, Adv. Funct. Mater. 23 (2013) 3549–3559.
[23] F.J. Uribe-Romo, J.R. Hunt, H. Furukawa, C. Klock, M. O'Keeffe, O.M. Yaghi, J. Am. Chem. Soc. 131 (2009) 4570–4571.
[24] A. Taha, B. El-Shetary, W. Linert, Monatsh. Chem. 124 (1993) 135–147.
[25] M.B. Hursthouse, K.M. Abdul Malik, D.M.P. Mingos, S.D. Willoughby, Organomet. Chem. 192 (1980) 235–251.
[26] J.I. Bullock, J. Inorg. Nucl. Chem. 29 (1967) 2257–2263.
[27] N.M. Karayannis, C.M. Mikulski, L.L. Pytlewski, M.M. Labes, Inorg. Chem. 13 (1974) 1146–1147.
[28] A. Taha, Synth. &React. Inorg. Metal. Org. 31 (2001) 205–218.
[29] A.A.T. Ramadan, M.A. El-Behairy, A.I. Ismail, M.M. Mahmoud, Monatsh. Chem. 125 (1994) 1171–1173.
[30] A.A.T. Ramadan, R.M. Abdel-Rahman, M.A. El-Behairy, A.I. Ismail, M.M. Mahmoud, Thermochim. Acta 222 (1992) 291–299.
[31] R.M. Silverstein, G.C. Bassler, T.C. Morrill, Spectrophotometric Identification of Organic Compounds, fourth ed., Wiley, New York, 1981.
[32] Y. Xiao, N. Cheng, K.K. Kondamareddy, C. Wang, X. Zhao, J. Power Sources 342 (2017) 489–494.
[33] L. Wang, W. Qin, X. Tang, W. Dou, W. Liu, Q. Teng, X. Yao, Org. Biomol. Chem. 8 (2010) 3751–3757.
[34] J.B. Asbury, Y.Q. Wang, Y.E. Hao, H. Ghosh, T. Lian, Res. Chem. Intermed. 27 (2001) 393–406.
[35] Z. Wu, B. Fan, F. Xue, C. Adachi, J. Ouyang, Energy Mater. Sol. Cells 94 (2010) 2230–2238.
[36] A. Gadisa, M. Svensson, M.R. Andersson, O. Inganas, Appl. Phys. Lett. 84 (2004) 1609–1611.
[37] H. Liu, V. Avrutin, N. Izyumskaya, Ü. Özgür, H. Morkoç, Superlattice Microstruct. 48 (2010) 458–484.
[38] J. Werner, R. Bergmann, in: Tech.Dig.12th Int. Photovoltaic Science and Engineering Conf.,Sapporo, 1999.
[39] K. Yamamoto, JSAP Int. 7 (2003) 12–19.
[40] N. Romeo, A. Bosio, V. Canevari, Inter. J. Sol. Energy 12 (1992) 183–186.
[41] B. Wang, Y. Cai, W. Dong, C. Xia, W. Zhang, Y. Liu, M. Afzal, H. Wang, B. Zhu, Sol. Energy Mater.Sol. Cells 157 (2016) 126–133.
[42] S. Mastroianni, F.D. Heinz, J.H. Im, W. Veurman, M. Padilla, M.C. Schubert, U. Würfel, M. Grätzel, N.G. Park, A. Hinsch, Nanoscale 7 (2015) 19653–19662.
[43] X. Liu, Y. Wu, Z. Li, Y. Gao, Appl. Surf. Sci. 400 (2017) 1–5.
[44] P.O. Edward, Hand Book of Optical Constants of Solids, Academic press, New York, 1985.
[45] J. Bardeen, F. Slat, L. Hall, in: Photoconductivity Conference, vol. 146, Wiley, New York, 1965.
[46] M.M. El-Nahass, E.M. El-Menyawy, Mater. Sci. Eng.B 177 (2012) 145–150.
[47] A. Taha, A.A.M. Farag, A.H. Ammar, H.M. Ahmed, Spectrochim. Acta Part A Mol. Biomol. Spectrosc. 122 (2014) 512–520.
[48] A.A.M. Farag, I.S. Yahia, F. Yakuphanoglu, M. Kandaz, W.A. Farooq, Opt. Commun. 285 (2012) 3122–3127.
[49] M.M. El-Nahass, H.M. Abd El-Khalek, A.M. NawarEur, Phys. J. Appl. Phys. 57 (2012) 30201–30314.
[50] Sawsan M.S. Haggag, A.A.M. Farag, M. Abdel Refea, Spectrochim. Acta Part A Mol. Biomol. Spectrosc. 102 (2013) 150–158.
[51] A. Ashery, A.A.M. Farag, M.A. Shenashen, Synth. Met. 162 (2012) 1357–1363.
[52] M. Dongol, M.M. El-Nahass, A. El-Denglawey, A.F. Elhady, A.A. Abuelwafa, Curr. Appl. Phys. 12 (2012) 1178–1184.
[53] A.U. Momin, A.P.B. Sinha, IETE J. Res. 9 (1963) 286–291.
[54] N. Dori, M. Menon, L. Kilian, M. Sokolowski, L. Kronik, E. Umbach, Phys. Rev. B 73 (2006) 195208–495214.
[55] H.M. Zeyad, M.M. El-Nahass, I.K. El-Zawawi, E.M. El-Menyawy, J. Phys. Chem. Solids 71 (2010) 867–875.
[56] J. Rouxel, Chem. Scr 28 (1988) 33.
[57] M. Dongol, M.M. El-Nahass, A. El-Denglawey, A.F. Elhady, A.A. Abuelwafa, Curr. Appl. Phys. 12 (2012) 1178–1184.
[58] A.A. AlGhamdi, A.A.M. Farag, A.A. Hendi, R.H. AlOrainy, F. El-Tantawy, F. Yakuphanoglu, Appl. Phys. A 121 (2015) 29–37.
[59] E.H. RhoderickMetal–Semiconductor ContactsClarendon, Oxford, 1978.
[60] S.M. Sze, Physics of Semiconductor Devices, second ed., John Wiley & Sons, New York, 1981.
[61] S. Kazim, V. Ali, M. Zulfequar, M.M. Haq, M. Husain, Phys. B 393 (2007) 310–315.
[62] M. Soylu, M. Cavas, A.A. Al-Ghamdi, Z.H. Gafer, F. El-Tantawy, F. Yakuphanogluc, Sol. Energy Mater. Sol. Cells 124 (2014) 180–185.
[63] M. Ravinandan, P.K. Rao, V.R. Reddy, J. Optoelectron, Adv. Mater. 10 (2008) 2787–2804.
[64] R.S. Ajimsha, K.A. Vanaja, M.K. Jayaraj, P. Misra, V.K. Dixit, L.M. Kukreja, Thin Solid Films 515 (2007) 7352–7356.
[65] S. Tataroglu, S. Altındal, J. Alloys Compd. 484 (2009) 405–412.
[66] I.S. Yahia, M. Fadel, G.B. Sakr, F. Yakuphanoglu, S.S. Shenouda, W.A. Farooq, J. Alloys Compd. 509 (2011) 4414–4419.
[67] K. Das, S.K. De, J. Lumin. 129 (2009) 1015–1022.
[68] Y. Wang, Sh. Yang, H. Wang, L. Zhang, H. Cheng, B. He, W. Li, B. Zou, Curr. Appl. Phys. 17 (2017) 343–350.